ACS NANO
Cite This: ACS Nano 2019, 13, 786−795
www.acsnano.org

ARTICLE

Molecular Identification, Bond Order Discrimination, and Apparent Intermolecular Features in Atomic Force Microscopy Studied with a Charge Density Based Method

Michael Ellner,[†] Pablo Pou,[†,‡] and Rubén Pérez*[,†,‡]

[†]Departamento de Física Teórica de la Materia Condensada, Universidad Autónoma de Madrid, E-28049 Madrid, Spain
[‡]Condensed Matter Physics Center (IFIMAC), Universidad Autónoma de Madrid, E-28049 Madrid, Spain

Supporting Information

ABSTRACT: We introduce an efficient method to simulate high-resolution atomic force microscopy (HR-AFM) images with CO probes. Our model explicitly takes into account the charge densities of the sample and the probe for the calculation of the short-range (SR) interaction and retains *ab initio* accuracy with only two parameters, that are essentially universal, independent of the number of chemical species and the complexity of the bonding topology. The application to molecular images shows a strong dependence on the stoichiometry and bonding configuration that precludes the chemical identification of individual atoms based on local force−distance curves. However, we have identified features in the 2D images and 3D force maps that reflect the highly anisotropic spatial decay of the molecular charge density and provide a way toward molecular identification. The model treats SR and electrostatics interactions on an equal footing and correctly pinpoints the Pauli repulsion as the underlying interaction responsible for the bond order discrimination in C60. Finally, we settle the controversy regarding the origin of the intermolecular features, discarding the effect of the charge redistribution associated with the H bonds, and linking them with the overlap of the wave functions of the atoms that constitute the bond. This overlap creates saddle regions in the potential energy landscape that are sensed by the probe.

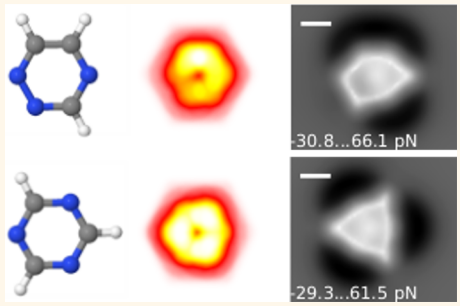

KEYWORDS: *non-contact atomic force microscopy, tip functionalization, CO molecule, chemical identification, bond order, hydrogen bonds, DFT*

Noncontact atomic force microscopy (NC-AFM) with metal tips functionalized with closed-shell molecules like CO and inert atoms as Xe has revolutionized the field of molecular imaging.[1] This technique, also referred to as high-resolution AFM (HR-AFM), is able to image the internal structure of molecules,[2] resolves features in the intermolecular regions of weakly bonded molecules,[3,4] discriminates between bond orders in aromatic compounds,[5] and has opened the door to following or even inducing on-surface chemical reactions.[6−8]

Theoretical models have helped to rationalize the imaging mechanisms of HR-AFM.[9] Density functional theory (DFT) analysis identified the short-range (SR) interaction, mainly Pauli repulsion, as the dominant interaction responsible for the imaging of molecular structures at small tip−sample distances.[2,10] DFT calculations, together with a model to calculate HR-AFM images that retain DFT accuracy, allowed the electrostatic (ES) charge distribution of CO-metal apexes[11] and its contribution to molecular imaging to be characterized.[12] Simpler and more computationally efficient methods, like the Particle-Probe (PP) model,[13] which describes the SR and vdW interactions through pairwise Lennard-Jones potentials[13] complemented with a point charge/multipole interacting with the full sample electrostatic field,[14] all parametrized to reproduce the experimental results, have helped us to understand how the flexibility of a molecular probe enhances the intra- and intermolecular contrast.[13−15] This approach[13] has become the main workhorse for HR-AFM simulations and has been applied to understand the role of the ES interaction in the imaging of molecules.[16−18]

In spite of these advances, there is still a strong debate regarding key issues in HR-AFM imaging. One of the important questions is the relative contribution of the different interactions to the AFM contrast. The first DFT based

Received: October 26, 2018
Accepted: January 3, 2019
Published: January 3, 2019

DOI: 10.1021/acsnano.8b08209
ACS Nano 2019, 13, 786−795

studies[2,5,10,19] as well as simpler models[20] attributed the most important origin of the observed features to the Pauli interaction. Later, Guo et al.[21] suggested that features associated with inter- and intramolecular bonds originate from the short-range electrostatic force. The success of the PP model[13] to accurately reproduce the experimental images has been used to deduce the origin and significance of the images. In many systems, image features are ruled by the Pauli repulsion modified by the ES field of the molecules, as correctly predicted by the PP model. However, in other cases, unveiling the origin contrast could be more difficult. For instance, in their analysis of bond order discrimination, Hapala et al.[22] simulated the features observed in the experimental images of the C_{60} molecule[5] by using, in addition to the Pauli repulsion, a very large effective charge for the CO probe, leading them to associate the bond order discrimination to the ES interaction, in spite of the nonpolarity of C60 molecules. Recent work,[23] also based in the PP model, has assigned a relevant role in the chemical discrimination on N and B decorated graphene nanoribbons to the van der Waals interaction, in contradiction to previous results that discard dispersion forces as the source of atomic contrast[10,24] due to the smoothness of the r^{-6} behavior.

There is also an on-going controversy about the ability of the AFM to disclose H-bonds. Intermolecular features have been observed with CO tips[3,13,18,25,26] and other inert tips.[4,27] However, their origin is still under debate. These features have been proposed to be a direct observation of the subtle charge redistribution associated with H-bonds[3] or attributed to an artifact due to the mobility of the probe.[15,28,29] An emerging consensus was linking this contrast to the spilling of the charge density of the molecules into the intermolecular region,[9,12,30] but a very recent work[31] with a rigid, passivated apex[32] has sparked again the debate.

An accurate understanding of the contrast and the role played by the different interactions in the AFM experiments is required to progress toward molecular identification.[1] HR-AFM imaging has already contributed to the structural elucidation of complex natural products,[33,34] polycyclic aromatic molecules like asphaltenes[35] and nanographene,[36] and on-surface reaction intermediates and products.[6,37−43]

The chemical identification of individual atoms with passivated probes is a more challenging task.[1] Chemical discrimination has been reported combining NC-AFM with other techniques such as Kelvin probe force microscopy[44−46] or scanning tunneling microscopy and DFT simulations.[1] NC-AFM measurements with reactive tips on semiconductor surfaces have shown that the chemical specie of individual atoms can be named through force spectroscopy measurements.[47,48] In this case, where both tip and sample are reactive, a covalent bond is formed between tip and sample atoms upon tip approach. Therefore, the interaction is highly dependent on the chemical specie of the two atoms,[47] being only slightly perturbed by the chemical environment. A similar mechanism cannot be expected to work in HR-AFM imaging of molecules involving nonreactive probes and samples.

A possible alternative for chemical identification of molecular systems is to find distinctive features in the images, or the 3D force maps, that could be associated with a particular atom irrespective of its chemical environment. Guo et al.[19] pointed out, from DFT calculations, that the replacement of one C−H group by a N atom in a pentacene molecule modifies the charge density and locally distorts the image, making the N substitutional distinct from the image of the remaining C atoms. These distortions have been observed in hydrocarbon rings with heteroatoms[42,49−51] and surfaces with dopants,[52] but it is still unclear what causes them.[9,16,22,50−55] Furthermore, 3D-force spectroscopy data on organic molecules obtained with CO probes exhibits a characteristic, local contrast that could be used for chemical recognition.[49] However, the possibility to get this atom by atom chemical identification with CO probes has been questioned as the contrast depends on the environment, hybridization, and oxidation state of the sample molecule.[1]

Here, we introduce a method for the simulation of HR-AFM images that contributes to answering these key issues. Our approach, merging ideas presented in previous works,[11,13,14,20] describes both the ES and SR interactions in terms of two physical observables: the total charge densities of the sample, ρ^{sample}, and the functionalized tip, ρ^{tip}, obtained from independent *ab initio* calculations. We replace, inspired by a simple way to account for the Pauli repulsion,[20] the pairwise fitting of the SR with Morse potentials previously used[11,12] by a function of the overlap of ρ^{tip} and ρ^{sample}, the physical quantity responsible for the Pauli repulsion, as

$$V_{\text{SR}} = V_0 \int [\rho^{\text{tip}}(\vec{r})\rho^{\text{sample}}(\vec{r})]^{\alpha}\, \mathrm{d}\vec{r} \tag{1}$$

This model, applied to a CO−metal tip, reproduces most of the features of HR-AFM images and retains DFT accuracy on molecules with multiple chemical species with just two parameters, V_0 and α, that are essentially universal. It clearly links bond order contrast with the Pauli repulsion and explains the origin of the intermolecular features, discarding the effect of the charge redistribution associated with the H-bonds. The model reveals a strong dependence of the molecular images on the stoichiometry and bonding configuration, which precludes the chemical identification of individual atoms based on local force−distance curves. However, it also identifies features in the HR-AFM images, linked to the presence of N substitutionals and in the 3D force maps, that reflect the spatial decay of the molecular charge density and provide a way toward the goal of molecular identification with the AFM.

RESULTS AND DISCUSSIONS

Contrast Formation of HR-AFM Images of a Pyridine Molecule. First, we illustrate the application of the method by simulating images of a pyridine molecule as probed by a CO tip (see Methods and Section S1 in the Supporting Information (SI) for a detailed description). A pyridine is a benzene ring in which an N atom substitutes a C−H group (see inset of Figure 1a). First, force curves are calculated with DFT on relevant sites of the molecule: the atoms, the middle point of the bonds, and the center of the ring. The force vs distance plot for a C atom (Figure 1a, solid blue line) shows a small attractive regime at large tip−sample distances ($z > 3.5$ Å) and a sharp repulsive one at smaller distances.

The total DFT interaction can be decomposed into its ES, vdW, and SR components. The first two, as described in the Methods section, are obtained from eq 3 and from a stand-alone DFT-D3[56] calculation. The SR component is isolated by subtracting the ES and vdW from the total interaction. The decomposed forces (Figure 1a) help to explain the different interaction regimes. At large distances, the attraction sensed by the tip mainly comes from the vdW interaction. At closer distances, the ES force with the CO probe provides an

DOI: 10.1021/acsnano.8b08209
ACS Nano 2019, 13, 786−795

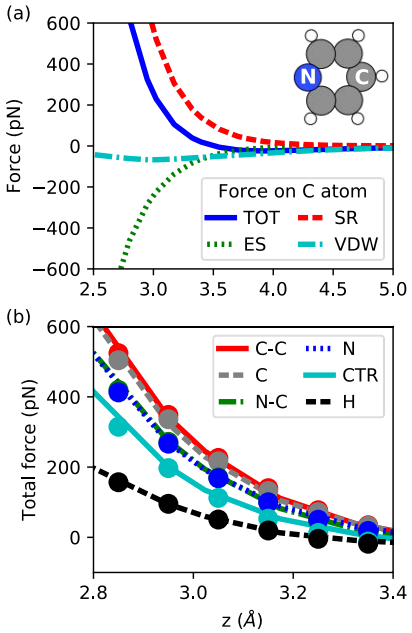

Figure 1. AFM spectroscopy of a pyridine molecule with a CO tip. (a) Force decomposition on the C atom opposite to the N atom. (b) Total force as calculated with DFT (lines) and the model (markers) for 6 sites. The C−C site is the midpoint between the C atom opposite to the N and a neighboring C atom. CTR is the center of the molecule. The fit, with a root-mean-square error (RMSE) of 6.1 pN, is very accurate.

attractive interaction. Although the electric field of the molecule is repulsive for negative charges (Figure S1 in the Supporting Information), the ES interaction, that includes the electron−electron, electron−ion, and ion−ion interactions, is attractive due to the overlap of the electronic charge densities (notice that once the electronic clouds overlap, the electronic and ionic electrostatic repulsion cannot screen completely the electron−ion attraction).[12] This overlap also causes the exponential growth of the Pauli repulsion. There is a strong cancellation between the SR and ES interactions,[12] which is finally won by the SR, leading to an increase of the repulsion as the tip−sample distance decreases.

We now apply our model to simulate HR-AFM images. In order to parametrize the SR interactions, we use the total force in all the sites shown in Figure 1b as solid lines. The C−C bond and the C atom are the most repulsive sites of the molecule, followed by the N−C bond and the N atoms. The least repulsive site is the H atom followed by the center of the molecule. For each force spectroscopy, the SR interaction is isolated as described in Methods. These data points are used to fit V_0 and α of eq 1 by minimizing the root-mean-square error (RMSE). Figure 1b shows the comparison of the forces as obtained with the model (circles) and DFT (lines) using the minimized parameters V_0 = 13.365 [eV] and α = 1.07 (notice that, as eq 1 is a power law, the fit parameters depend nontrivially on the unit of the charge density; here, all charge densities are in e/Å^3 and energies in eV, and we use [eV] to depict this unit choice). For these tip−sample distances, typical for the experimental HR-AFM images, the model agrees extremely well with the DFT calculations, yielding a RMSE of 6.1 pN in a force range of more than 600 pN. Note that the exponential factor of eq 1, α, is only slightly larger than one. In other words, the functional form of the SR interaction is almost the pure overlap of the electronic charge densities.

Having obtained a proper fit, AFM maps of the molecule are simulated by calculating the interaction on a 2D grid (see Methods and Section S1). Taking advantage of the capability of the model to separate the different contributions to the total force, the interaction-decomposed force maps for a tip height (referred to the oxygen position in the CO probe) of z = 3.1 Å above the molecular plane are plotted in Figure 2 with a rigid CO tip (static map) along with the force gradient map for a flexible tip (relaxed map), which in the small amplitude limit, is proportional to the frequency shift.[57] The strong cancellation between the SR and ES maps plus the addition of a weak vdW attraction results in a static force map that has an asymmetrical hexagonal shape (the atomic geometry has the N atom and C−H groups arranged in a hexagon), with a dark hollow center and a darker halo around the molecule. The hollow center in the total force map is a direct consequence of the SR interaction. This contribution is very local, and thus, it is stronger when the tip is placed on top of a single atom compared to the center of the molecule. In contrast, the vdW interaction, which has a longer range, makes the center to be slightly darker, and is also responsible for the dark halo around the molecule.[2]

These force maps clearly show, in agreement with the force curves, that the C sites are more repulsive than the N site, leading to a distorted image compared to the almost perfect hexagonal structure. This difference stems mainly from the SR interaction, with a small contribution from the ES force that is a bit less attractive on the N site compared to the C atoms. Considering the number of valence electrons, one could naively expect a greater repulsion on the N site. Our analysis of the different 6-membered rings with different number of N atoms will explain this apparent paradox highlighting the role of the spatial decay of the charge density in the observed contrast.

The asymmetry of the total interaction map is not only limited to the difference in force between the C and N atoms but also to the locations of their respective maxima, with the N

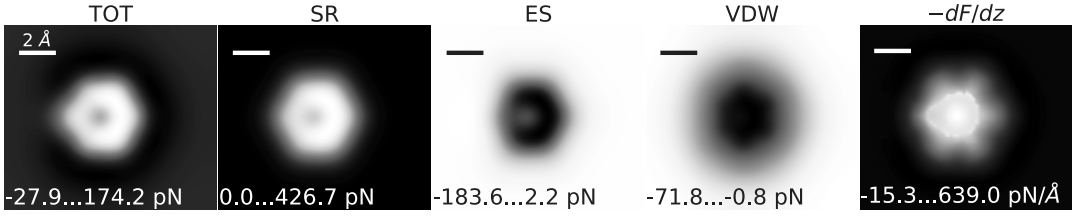

Figure 2. Constant height AFM images of the pyridine molecule calculated with the model. From left to right: static total, short-range, electrostatic, and van der Waals forces and the total force gradient (proportional to the frequency shift) with tip relaxation. Tip height, from the molecular plane to the oxygen in the CO probe, of z = 3.1 Å.

DOI: 10.1021/acsnano.8b08209
ACS Nano 2019, 13, 786−795

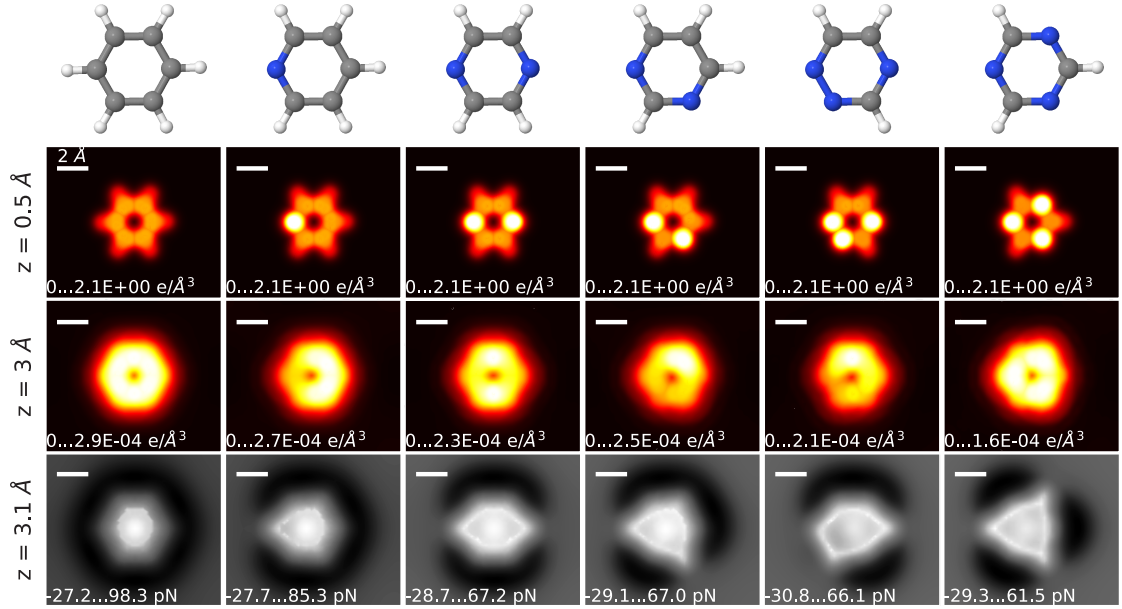

Figure 3. Six-membered rings with N heteroatoms. From left to right: benzene, pyridine, pyrazine, pyrimidine, 1,2,4-triazine, and an s-triazine. From top to bottom: schematic representation of molecules, charge density at 0.5 and 3 Å from the plane of the molecule, and total force maps (including the effect of CO tilting) at z = 3.1 Å.

atom having a slightly more extended vertex than the C−H groups. The flexibility of the CO tip enhances this effect in the force gradient (frequency shift) image by sharpening the saddle lines of the static map. These asymmetries are typically observed in experimental images.[42,49−51] Notice that models that describe the repulsion with pairwise potentials,[9,16,22,50−55] including our previous Morse based approach,[11,12] tend to produce more rounded shapes and have a hard time reproducing these features. The sharper vertex associated with the N atom is not unique to this molecule and can be explained in terms of the lateral extension of the lone-pair orbital of the N atom. Below, we discuss how this feature can help with the molecular recognition.

Molecular Identification: 6-Membered Rings. Here we explore whether the differential features associated with the N atoms can be used as the basis for molecular identification, comparing the theoretical images produced with our model for benzene, pyridine (with one N heteroatom), and the rest of the N atom 6-membered heterocyclic compounds (see the first row of Figure 3): pyrazine and pyrimidine (both with two N heteroatoms) and 1,2,4-triazine and 1,3,5-triazine (hereafter s-triazine), both with three heteroatoms. The corresponding force maps, simulated with our model (including the CO tip tilt) for a tip−molecule distance z = 3.1 Å, are displayed in the last row of Figure 3. The optimized system-specific parameters (V_0 and α) have very similar values (see Table 1).

The counterintuitive N−C asymmetry in the force maps of pyridine described above is also present in the rest of the molecules, and it can be easily explained by examining the corresponding charge density. The N atom, having more valence electrons than the C atoms, have a larger charge density close to the plane of the molecule (second row of Figure 3). However, the charge density of the N atom has a faster decay with the distance than the one of the C atoms, resulting in a smaller contribution to the total charge density at the z = 3 Å plane (Figure 3, third row). At this plane, the charge density accumulates in the C−C bonds because the associated π orbitals decay slower and have greater extension than those for the N−C (and N−N) bonds, making them, and the C sites, more repulsive than the N atom due to the overlap with the CO's wave function. s-Triazine, lacking C−C bonds, breaks this rule: even at z = 3 Å, the charge densities of the N atoms remain larger (decay slower) than the ones of the C atoms. This is a consequence of the nature of the molecular orbitals, which are determined not only by the stoichiometry but also by the molecular bonding structure. This is most evident in the pyrimidine molecule which has three C atoms with C−C bonds and one C atom without. The latter has the smaller charge density, even compared to the two N atoms (Figure 3), and exerts the weakest repulsive force (Figure S2). This behavior could be difficult to observe in the frequency shift images due the CO tilting but is exposed in the information derived from 3D maps.[49]

Table 1. Parameters Fitted To Reproduce the DFT Results for the SR Interaction Using Equation 1[a]

molecule	V_0 [eV]	α (system)
benzene	14.484	1.08
pyridine	13.365	1.07
pyrazine	13.534	1.07
pyrimidine	13.549	1.07
1,2,4-triazine	13.725	1.07
s-triazine	15.221	1.08
universal parameters	13.928	1.073
Breitfussin A	12.413	1.07
C60	13.491	1.07
8-hq tetramer	21.826	1.12
8-hq dimer	22.012	1.12

[a]The universal parameters are an average of those obtained for the 6-membered rings including a different number of N atoms (see the top panel of Figure 3. In the case of the 8-hq tetramer (dimer), four (five) intermolecular sites (see Figures S4 and S5) are included in the fitting in order to reproduce accurately the subtle PES for the CO probe on that region.

DOI: 10.1021/acsnano.8b08209
ACS Nano 2019, 13, 786−795

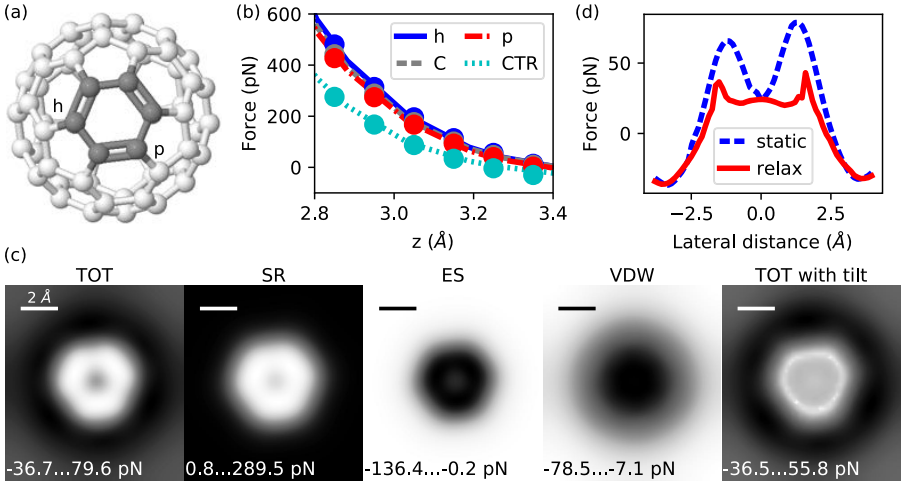

Figure 4. Simulated images of a C60 molecule which has distinct bond orders. (a) Schematic representation of the molecule with the hexagon facing upward. (b) Total force calculated with DFT (lines) and the model (markers) for four positions. The h position is for the bond fusing two hexagons, and the p position is for the bond fusing a pentagon and a hexagon; the h bond has a larger bond order than the p bond. CTR is the center of the hexagon. (c) Force maps for z = 3.2 Å. From left to right: static total, short-range, electrostatic, and van der Waals and the total force with a flexible tip. With the model, bond order discrimination obtained with a CO tip is attributed to the short-range interaction. (d) Force profiles along the line passing through the p and h bonds with the CO tip fixed in the upright position (dashed blue line) and allowed to relax (solid red line).

Although the N−C repulsive asymmetry seems to be very much dependent on the stoichiometry and bonding configuration, there is a feature that can be associated with the electronic configuration of the N: As in pyridine, the rest of the N heteroatom 6-membered rings' AFM images have sharper vertices around the N atoms as compared to the C−H groups (Figure 3, bottom row). Far from the plane of the molecule (z = 3 Å), the charge density associated with the N lone pair overflows laterally more than the C−H groups. This overflow, in turn, originates a repulsive electric field around the N (see Figure S1), is reflected slightly on the SR interaction, and is clearly marked on the ES contribution. The strong SR-ES cancellation leaves a Potential Energy Landscape (PES) whose saddle lines connect past the N atoms and deform the hexagonal symmetry of the molecules. The tip tilt, which emphasizes the saddle lines of the PES, highlights the asymmetry of the charge density around the N atoms. These features, which depend on subtle details of the total charge density, are hard to capture with a pairwise description of the SR interaction. Thus, both the 3D force maps and the sharper vertices disclosing the location of the N atoms in the AFM images provide a fingerprint for the studied molecules.

Bond Order Discrimination: C60 Molecule. Our method is able to pick up differences in the order of covalent bonds directly as a collective property of the charge density. We demonstrated this on the Buckminsterfullerene (C60), a molecule with 20 hexagons and 12 pentagons with C atoms on each vertex (see Figure 4a). The structural asymmetry of the C arrangement induces alternating single C−C bonds at the links between two hexagons (h) and double C−C bonds at the links between hexagons and pentagons (p).

DFT force curves on a C atom, a single bond (p), a double bond (h), and the center of the hexagon (CTR) were used to determine the two parameters defining the SR interaction in the model. Figure 4b shows a comparison between the model (circles) and DFT calculations (lines). The minimized parameters, V_0 = 13.491 [eV] and α = 1.07, are again very close to those found for the molecules discussed in the previous section and reproduce extremely well the DFT results (with a RMSE = 6.6 pN). Already from the force spectroscopy (Figure 4b), it is clear that the double bond exerts a greater repulsion on the probe than both the C atom and the single bond, with the least repulsive site at the center of the hexagon.

The static force maps at z = 3.2 Å (Figure 4c) confirm that the higher repulsion of the h position is distributed along the whole bond (line joining the C atoms), breaking the hexagonal symmetry and leading to an image with triangular shape with vertices on the h positions. Although there is a strong cancellation between the SR and ES interaction, the former is clearly responsible for the shape of the static map. However, the ES interaction induces lateral distortions[17] to the saddle lines of the PES created by the SR. The relaxation of the CO probe (last panel in Figure 4c) highlights the saddle lines in the PES and shortens the distance of the double bond compared to the single bond.[5] Although the tilt slightly saturates the total force along the bonds, the h position remains more repulsive than the p position. This can be clearly seen in Figure 4d where profiles at z = 3.2 Å, going from the p to the h position, are plotted for the two cases: the CO probe kept fixed (static) and allowed to tilt (relax). The asymmetric shape of the C60 image is not only due to the Pauli repulsion: apparent bonds are shifted outward from the center by the ES forces,[17] enhancing the difference in the apparent distances (see Figure S3).

These results are fully consistent with the experimental discrimination of bond orders on the C60 molecule[5] and prove unambiguously that the SR contribution, through the charge density of the sample, is crucial for the discrimination. Bond order discrimination and the sharper vertices leading to chemical identification within a molecule described above are inextricably linked to the subtle spatial modulation of the sample charge density and, thus, cannot be naturally captured with pairwise descriptions of the SR interaction.[11,13] In order to reproduce the bond orders or differences between the same chemical specie in different molecular environments, they have to either increase the number of parameters, including for example extra ghost atoms, as we did in our previous DFT-

DOI: 10.1021/acsnano.8b08209
ACS Nano 2019, 13, 786−795

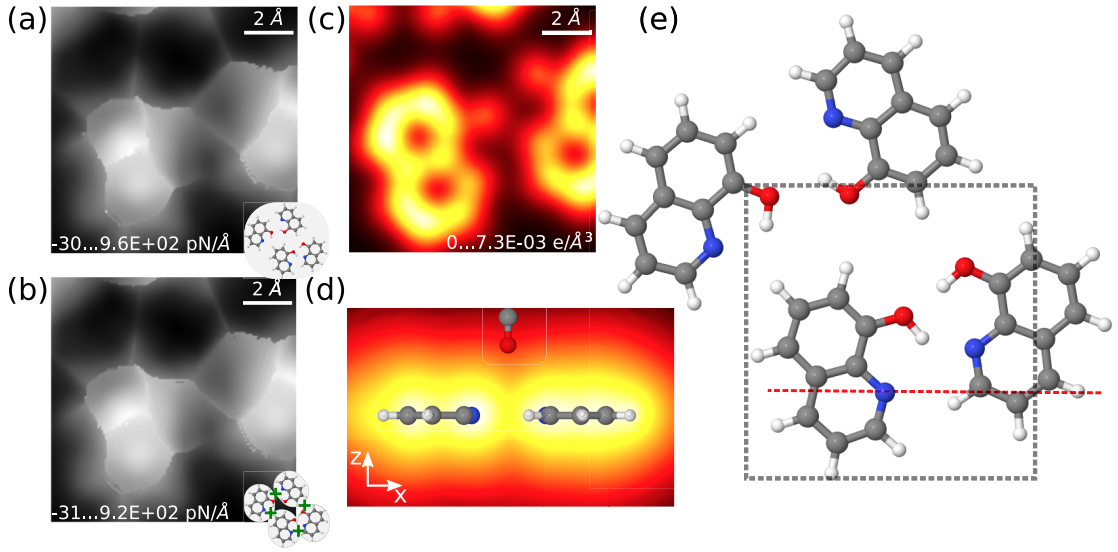

Figure 5. Simulated images of an 8-hq tetramer. (a) Force gradient map at z = 3.04 Å for the region marked in (e). (b) Force gradient map (at the same height and area as (a)) for an ideal system built as the sum of the four isolated molecules, where, by construction, there is no charge redistribution induced by the H-bond formation. Charge density (c) at a plane 3.04 Å above the molecule; and (d) in the z–x plane along the H-bond marked by a red line in (d). (e) Ball-and-stick representation of the 8-hq tetramer. The intermolecular contrast of the AFM images is due to the overlap of the wave functions of O, N, C, and H atoms with no enhancement due to the formation of H-bonds.

based approach,[12] or bluntly modify other force contributions, twisting the vdW interaction or assuming a large net charge on the CO–metal tip to increase the ES contribution,[22] as done with the parametrized PP model. At variance with this, our method is able to model these subtle collective effects coming from the total sample charge density.

Imaging H-Bonds: 8-hq. Given the success of our model in reproducing and explaining the subtle contrast associated with the bond orders in terms of the total charge density, we tackle the controversy regarding the origin of the intermolecular features observed when imaging molecules that support H-bonds.[3,9,12,13,15,25,30,31]

To this end, we study the 8-hydroxyquinoline (8-hq) tetramer.[3] First, we will demonstrate that, by giving weight in the fitting to the intermolecular region, our method is able to reproduce the DFT tip–sample interactions in those areas. In order to fit the two parameters (V_0 and α) that describe the SR interactions, we have included several sites that we would use to describe an isolated 8-hq molecule (on top of the O, N, C, and H atoms, the middle of the O–C bond, and the centers the rings) plus four additional sites in the intermolecular region: two sites along H-bonds and two sites between H-bonds (Figure S4). Our model with the fitted SR parameters (V_0 = 21.826 [eV], α = 1.12) provides an excellent description (RMSE = 4.7 pN) of the DFT force curves (Figure S5), both in the intra- and intermolecular regions. In particular, it reproduces an energy profile along a line transverse to H-bonds (Figure S6c) with an accuracy better than 1 meV. Our simulated AFM image for the 8-hq tetramer (including the CO tilt) clearly shows the silhouette of the two rings and the OH group of each molecule, as well as the intermolecular features associated with the H-bonds (Figure 5a). These features are fainter than the lines highlighted by the CO tilt across the aromatically bonded atoms. These results are consistent with experimental images.[3]

To explain the origin of the intermolecular features observed in the experiments, we first examine the charge density of the sample. Figure 5c presents a slice of the charge density at a plane z = 3.04 Å above the hq-8 tetramer. Areas of larger charge density can be observed along the zones joining the molecules through the lines connecting O, N, or C atoms. It is important to notice that these are precisely the lines O···O, O···N, and N···C that show up in the AFM image (see Figure S6a) and not the ones joining the H's with O or N atoms. The important question is whether they are due to the charge redistribution that occurred in the formation of the H-bonds or they simply reflect the sum of charge densities of the isolated molecules.

To discard the thesis of direct H-bond observation in HR-AFM, we compared images obtained with our model for the 8-hq tetramer (Figure 5a) and for a fictitious system where the charge density of the four molecules was obtained from DFT calculations for four isolated molecules and then added together (Figure 5b). The proximity of the two molecules marked by a rectangle in Figure 5e, with an O–H···O distance of ∼1.7 Å, induces a non-negligible charge redistribution (see Figure S7). This redistribution is not only happening at the molecular plane (z = 0)—a region not accessible to the CO probe—but also at the height where the CO is placed, z ∼ 3 Å, where, in fact, electrons are expelled out from the intermolecular area (see Figures S6b and S7). Consequently, the effect of the charge redistribution would be to make the interaction with the CO slightly less repulsive (Figure S6c). However, this effect does not reflect in the AFM image (see the force gradient profile in Figure S6d). Figure 5b shows the simulated AFM image of the fictitious system formed by the sum of the four isolated molecules. There are not appreciable differences with the image of the real 8-hq tetramer (Figure 5a).

So far, we have focused on the intermolecular area where the charge redistribution associated with the formation of the H-bonds is more important. It is significantly smaller, <5%, in other areas where molecules are not so close. This is also the case for an 8-hq dimer (see Figures S4 and S8), where the H-bond distance is much larger, ∼2.8 Å, and the intermolecular features fainter precisely due the large separation, which

DOI: 10.1021/acsnano.8b08209
ACS Nano 2019, 13, 786–795

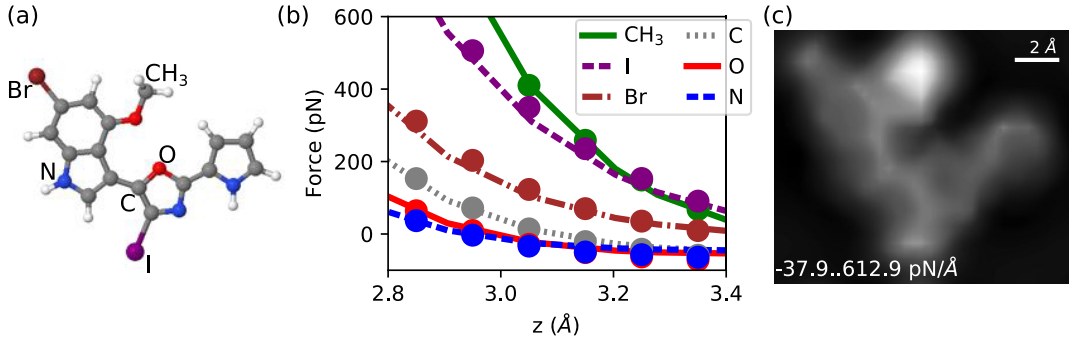

Figure 6. Simulated images of a Breitfussin A molecule which has six distinct atomic species. (a) Schematic representation of the molecule. (b) Total force as calculated from DFT (lines) and the model (markers) on six sites. (c) Force gradient (proportional to the frequency shift) image simulated with the model at z = 3.1 Å showing a striking resemblance with experimental images reported in ref 34.

reduces the overlap of the charge density of the molecules. At the height where the probe is placed, the charge density in both the tetramer and the dimer is controlled by the more delocalized molecular orbitals that extend into the intermolecular region (see Figure 5c,d). Thus, the features in the intermolecular region are induced by the same charge density that is responsible for the intramolecular contrast through its spatial decay in the outer regions of the molecule.[30] In summary, our results conclusively show that the charge redistribution has, if any, a very minor and certainly unexpected role. In the 8-hq tetramer, it would tend to reduce the contrast of the interatomic features, as the redistribution leads to a reduction of the electronic density at the intermolecular areas close to the probe.

Can the Model Deal with Many Different Chemical Species and Nonplanar Geometries? Universal Parameters. After the success in reproducing the intra- and intermolecular contrast for aromatic molecules including C, N, and O and the bond order in C_{60}, it seems natural to consider the performance of our model for more complex atomic geometries and a larger number of different chemical species. To this end, we examine the Breitfussin A (BfA) molecule (see Figure 6a), a halogenated natural product that contains six different chemical species (including the halogens Br and I) and whose structure has been determined with the assistance of AFM experiments.[34] BfA has a polar charge distribution and adopts a nonplanar geometry upon adsorption on a metal substrate, due particularly to the CH_3 group, what makes it an ideal candidate to test the capabilities of our model.

In order to simulate the HR-AFM image, the atomic positions of the molecule were obtained by relaxing the molecule on top of the Cu(111) substrate used in the experiments[34] (see Section S1 in the Supporting Information for details). DFT calculations for the tip−sample interaction on top of atoms of the different chemical species, the middle point of the bonds, and the center of the rings were used to parametrize the model. Figure 6b shows the excellent agreement between the DFT forces (lines) and the ones produced by the model (circles) for a representative subset of these sites. The simulated force gradient (proportional to the frequency shift, Figure 6c) is strikingly similar to the experimental images,[34] showing the CH_3 as the brightest feature, the faint silhouette of the rings, and an elongated oval around the I atom. However, because the molecule is kept frozen in the simulations, the repulsion of the CH_3 group is overestimated, reducing the overall contrast on the rest of the features.

The results for BfA confirm that our proposal to describe the SR interaction is capable of dealing with different chemical species and atomic geometries with no need to account for them explicitly in the formulation. Whereas our pairwise SR model based on Morse potentials[11,12] would need at least 18 parameters (3 × the number of species) to reproduce the tip−sample interaction, the model retains DFT accuracy with only two parameters irrespective of the number of species. Furthermore, the SR parameters fitted for this complex molecule (V_0 = 12.413 [eV] and α = 1.07) are very similar to the ones obtained for the molecules considered in the previous sections (see Table 1).

This striking similarity suggests the possibility of using the same universal V_0 and α parameters on all the molecules, eliminating the need for the computationally costly SR fitting. Moreover, for a given tip, ρ^{tip} only needs to be calculated once, and the model would only require the ρ^{sample} and ϕ^{sample} of the isolated sample. With this perspective, our method requires the same computational effort as in the Tersoff-Hamann approximations used to simulate scanning tunneling microscopy (STM) images—where ρ^{sample} is the only required *ab initio* input for a calculation—but retains DFT accuracy in the description of HR-AFM images.

To test this possibility, we have revisited the N heteroatom 6-membered rings and simulated images using the universal parameters V_0 = 13.928 [eV] and α = 1.073 obtained by averaging the SR parameters for all of these molecules. Figure S9 shows a comparison of static force vs distance plots and static force maps simulated using system-specific parameters and universal parameters for benzene, pyridine, and s-triazine. The force curves obtained with the universal parameters agree quantitatively with the DFT calculations: The average of the RMSE for all of the 6-membered rings increases from 7.3 pN when using the system-specific parameters to just 12.0 pN with the universal parameters. Likewise, there are no appreciable differences between the static force maps obtained from the two sets of parameters. The same results are obtained for the 8-hq tetramer and dimer (see Figure S8), where the system-specific parameters, fitted to reproduce the subtle features in the intermolecular region, deviate more from the universal parameters. While α deviates less than 5% from the values used for the rest of the molecules studied in this article (see Table 1), a significantly larger V_0 is needed in order to reproduce the subtle PES in the intermolecular area (see Figure S8). Nevertheless, this combination of parameters does not spoil

DOI: 10.1021/acsnano.8b08209
ACS Nano 2019, 13, 786−795

the description of the intramolecular contrast. These results support the ability of our model with universal parameters to simulate HR-AFM images and to describe the SR interaction between the sample and closed-shell probes with DFT accuracy.

CONCLUSIONS

We have developed an efficient method to simulate HR-AFM images with DFT accuracy that only requires two independent *ab initio* calculations for the tip and sample to determine the corresponding charge density and electrostatic potential. Our approach decomposes the total interaction into ES, vdW and SR contributions and accounts for the mobility of a flexible probe. The SR component is calculated from the overlap of the charge densities of the tip and the sample with a functional form that only has two parameters, that are essentially universal, independent of the number of different chemical species and the complexity of the bonding topology, including nonplanar geometries. Our model describes with high accuracy both the intra- and intermolecular features in HR-AFM images and links them with the spatial decay of the charge density into the area where the tip is placed.

Using this method, we have contributed to three of the main open issues in HR-AFM imaging. Our study of 6-membered rings with different numbers of N substitutionals has shown that the molecular images are very sensitive not only to the stoichiometry of the molecule but also to the bonding structure, with the most repulsive regions being located either on the C or the N atoms. This dependence on the chemical environment precludes a simple extension of the approach based on the properties of force−distance curves on individual atoms developed for chemical identification with reactive tips. However, our results show that the combination of 3D force maps with certain features in the 2D images, like differences in the vertex structure that are highlighted by the CO tip, can be used for the chemical identification of small molecules and specific groups of atoms or moieties within a complex system. These properties emerge from the electronic structure of the molecule and act as a fingerprint of the associated molecular charge density. They provide a method in the definition of a protocol for a complete identification of the structure and composition of molecular systems.

Our AFM simulations on C60 not only reproduce the experimental images but also pinpoint the SR as the crucial interaction for the bond order discrimination, which is enhanced by the ES lateral forces. Lastly, we settle the controversy present in the literature regarding the mechanisms that are responsible for the imaging of the intermolecular features. The charge redistribution associated with the formation of the H-bond is, usually, small and mostly localized on the molecular plane. But, even in cases where it is not negligible and distorts the total charge density in the areas accessible to the CO tip, it does not significantly modify the AFM image. This leaves the overlap of the wave functions of the atoms that are involved in the H-bond as the source of repulsion that generates a PES whose saddle lines are highlighted by the mobility of the probe. Thus, it is the intrinsic structure of the PES, controlled by the spatial decay of the charge density, that leads to the appearance of the intermolecular features in NC-AFM images.

METHODS

We have developed a new approach to simulate HR-AFM interaction-decomposed images that is based on the total charge densities of the tip and the sample, ρ^{tip} and ρ^{sample}, and the electrostatic potential of the sample ϕ^{sample}, obtained from two independent *ab initio* calculations. The method is computationally efficient, has only two parameters (that are essentially universal), and retains DFT accuracy in the description of the tip−sample interaction. Following our previous model,[11,12] the tip−sample interaction is decomposed into electrostatic (ES), short-range (SR), and van der Waals (vdW) components, while the mobility of the probe is accounted for through a restoring harmonic potential.[13] For a given tip's initial position $\vec{R}_{tip}$, the probe's relaxed coordinate is obtained by minimizing the potential

$$V(\vec{R}_{tip}, \theta, \varphi) = V_{ES} + V_{SR} + V_{vdW} + V_{tilt} \quad (2)$$

with respect to the tilt polar θ and azimuth ψ angles.

The ES, vdW and tip tilt potentials are calculated with the same functional form used in our previous model.[11,12] The ES interaction is computed from the overlap of ϕ^{sample} and ρ^{tip}. Notice that ϕ^{sample} includes the ES potential of both sample electron clouds and ions, while ρ^{tip} is the total charge density of the tip, including both electrons and ions. Therefore, the total ES interaction is

$$V_{ES} = \int \rho^{tip}(\vec{r}, \vec{R}_{tip}, \theta, \varphi)\phi^{sample}(\vec{r})\, d\vec{r} \quad (3)$$

The vdW interaction is obtained using Grimme's DFT-D3 approach[56] and the probe's tilt energetic penalty V_{tilt} through a restoring potential. For the CO tip with polar symmetry, it has the form of a torsion spring

$$V_{tilt} = \frac{1}{2}\kappa\theta^2 \quad (4)$$

A spring constant κ = 0.01 Ha/rad^2 seems best to reproduce experimental results.[11−14,58]

Here, we take a new approach to the SR interaction and use a description based on the charge densities of the tip and the sample that put this interaction on equal footing to the ES interaction. With the separation of the interaction given in eq 2, the SR contribution is basically originated by the Pauli repulsion in the tip−sample distance range relevant for the experiments. We have incorporated the charge density of the tip into the idea proposed by Moll et al.[20] that the Pauli repulsion is proportional to a power of the charge density of the sample[20] by calculating the SR as a function of the overlap of ρ^{tip} and ρ^{sample}:

$$V_{SR} = V_0 \int [\rho^{tip}(\vec{r}, \vec{R}_{tip}, \theta, \varphi)\rho^{sample}(\vec{r})]^{\alpha}\, d\vec{r} \quad (5)$$

The two SR parameters, V_0 and α, can be fitted with input data coming from DFT force curves of the most relevant sites of the sample. This functional form provides an excellent description of the DFT results with two parameters that are essentially universal (see Table 1), independent of the number of chemical species and the bonding topology.

An isolated CO molecule was used as a model for a CO-functionalized metal tip. In these tips, the metallic cluster is separated >3 Å from the imaged molecule and does not contribute toward the SR interaction contrast. Due to its long-range character, the vdW contribution of the metallic cluster provides negligible atomic contrast. This is also the case for the ES interaction, where only features with a large spatial separation compared with the interatomic distance will be resolved. A metallic tip generates an electric field, that can be well described by a positive electric dipole at the tip apex, with a large spatial extension that averages out the ES contributions of charges that vary on the atomic scale.[11]

Our new approach provides a realistic, accurate description of the HR-AFM images and offers insight into the nature of the interaction between a closed-shell tip and the sample, using as the main input data only 3D scalar fields: ρ^{tip}, ρ^{sample}, and ϕ^{sample}. We have calculated these magnitudes using the VASP[59] code, but they can be easily

DOI: 10.1021/acsnano.8b08209
ACS Nano 2019, 13, 786−795

accessed from all the standard DFT packages with a single, fast calculation. Our DFT calculations were carried out with the projector augmented-wave (PAW) method implemented in VASP, using the PBE exchange and correlation (XC) functional[60] supplemented by vdW DFT-D3.[56] We have used a 600 eV plane-wave cutoff and a 10^{-6} eV accuracy for the electronic self-consistency loop (see Section S1A in the Supporting Information for details).

Regarding the AFM calculations, a 2D energy map is obtained by evaluating the tip−sample potential (eq 2) on a grid (see Section S1B). Force maps are calculated from the first derivative with respect to the z direction of eq 2 and, in the small oscillation regime, frequency shift maps from the second derivative.[57]

ASSOCIATED CONTENT

Supporting Information

The Supporting Information is available free of charge on the ACS Publications website at DOI: 10.1021/acsnano.8b08209.

Further details concerning the simulations, the forces, and electric field on the 6-membered heterocyclic compounds; the effect of the electrostatic interactions in the bond order imaging on the C_{60} molecules; forces, differential charge densities, and charge and interaction profiles for the 8-hq tetramer; and the comparison of images calculated with our model using either system-specific or universal parameters for the 8-dimer and the 6-membered heterocyclic compounds (PDF)

AUTHOR INFORMATION

Corresponding Author

*(R.P.) E-mail: ruben.perez@uam.es.

ORCID

Pablo Pou: 0000-0002-5854-8218

Rubén Pérez: 0000-0001-5896-541X

Notes

The authors declare no competing financial interest.

ACKNOWLEDGMENTS

We are grateful for the financial support from AEI/FEDER under Project MAT2017-83273-R and from MINECO under Projects MAT2014-54484-P and MDM-2014-0377.

REFERENCES

(1) Gross, L.; Schuler, B.; Pavliček, N.; Fatayer, S.; Majzik, Z.; Moll, N.; Peña, D.; Meyer, G. Atomic Force Microscopy for Molecular Structure Elucidation. *Angew. Chem., Int. Ed.* **2018**, *57*, 3888−3908.

(2) Gross, L.; Mohn, F.; Moll, N.; Liljeroth, P.; Meyer, G. The Chemical Structure of a Molecule Resolved by Atomic Force Microscopy. *Science* **2009**, *325*, 1110−1114.

(3) Zhang, J.; Chen, P.; Yuan, B.; Ji, W.; Cheng, Z.; Qiu, X. Real-Space Identification of Intermolecular Bonding with Atomic Force Microscopy. *Science* **2013**, *342*, 611−614.

(4) Sweetman, A. M.; Jarvis, S. P.; Sang, H.; Lekkas, I.; Rahe, P.; Wang, Y.; Wang, J.; Champness, N. R.; Kantorovich, L.; Moriarty, P. Mapping the Force Field of a Hydrogen-Bonded Assembly. *Nat. Commun.* **2014**, *5*, 3931.

(5) Gross, L.; Mohn, F.; Moll, N.; Schuler, B.; Criado, A.; Guitian, E.; Peña, D.; Gourdon, A.; Meyer, G. Bond-Order Discrimination by Atomic Force Microscopy. *Science* **2012**, *337*, 1326−1329.

(6) de Oteyza, D. G.; Gorman, P.; Chen, Y.-C.; Wickenburg, S.; Riss, A.; Mowbray, D. J.; Etkin, G.; Pedramrazi, Z.; Tsai, H.-Z.; Rubio, A.; Crommie, M. F.; Fischer, F. R. Direct Imaging of Covalent Bond Structure in Single-Molecule Chemical Reactions. *Science* **2013**, *340*, 1434−1437.

(7) Albrecht, F.; Pavliček, N.; Herranz-Lancho, C.; Ruben, M.; Repp, J. Characterization of a Surface Reaction by Means of Atomic Force Microscopy. *J. Am. Chem. Soc.* **2015**, *137*, 7424−7428.

(8) Pavliček, N.; Gross, L. Generation, Manipulation and Characterization of Molecules by Atomic Force Microscopy. *Nat. Rev. Chem.* **2017**, *1*, 0005.

(9) Jelínek, P. High Resolution SPM Imaging of Organic Molecules with Functionalized Tips. *J. Phys.: Condens. Matter* **2017**, *29*, 343002.

(10) Moll, N.; Gross, L.; Mohn, F.; Curioni, A.; Meyer, G. The Mechanisms Underlying the Enhanced Resolution of Atomic Force Microscopy with Functionalized Tips. *New J. Phys.* **2010**, *12*, 125020.

(11) Ellner, M.; Pavliček, N.; Pou, P.; Schuler, B.; Moll, N.; Meyer, G.; Gross, L.; Pérez, R. The Electric Field of CO Tips and Its Relevance for Atomic Force Microscopy. *Nano Lett.* **2016**, *16*, 1974−1980.

(12) Ellner, M.; Pou, P.; Pérez, R. Atomic Force Microscopy Contrast with CO Functionalized Tips in Hydrogen-Bonded Molecular Layers: Does the Real Tip Charge Distribution Play a Role? *Phys. Rev. B: Condens. Matter Mater. Phys.* **2017**, *96*, 075418.

(13) Hapala, P.; Kichin, G.; Wagner, C.; Tautz, F. S.; Temirov, R.; Jelínek, P. Mechanism of High-Resolution STM/AFM Imaging with Functionalized Tips. *Phys. Rev. B: Condens. Matter Mater. Phys.* **2014**, *90*, 085421.

(14) Hapala, P.; Temirov, R.; Tautz, F. S.; Jelínek, P. Origin of High-Resolution IETS-STM Images of Organic Molecules with Functionalized Tips. *Phys. Rev. Lett.* **2014**, *113*, 226101.

(15) Hämäläinen, S. K.; van der Heijden, N.; van der Lit, J.; den Hartog, S.; Liljeroth, P.; Swart, I. Intermolecular Contrast in Atomic Force Microscopy Images without Intermolecular Bonds. *Phys. Rev. Lett.* **2014**, *113*, 186102.

(16) Van Der Lit, J.; Di Cicco, F.; Hapala, P.; Jelínek, P.; Swart, I. Submolecular Resolution Imaging of Molecules by Atomic Force Microscopy: The Influence of the Electrostatic Force. *Phys. Rev. Lett.* **2016**, *116*, 096102.

(17) Hapala, P.; Švec, M.; Stetsovych, O.; van der Heijden, N. J.; Ondráček, M.; van der Lit, J.; Mutombo, P.; Swart, I.; Jelínek, P. Mapping the Electrostatic Force Field of Single Molecules from High-Resolution Scanning Probe Images. *Nat. Commun.* **2016**, *7*, 11560.

(18) Peng, J.; Guo, J.; Hapala, P.; Cao, D.; Ma, R.; Cheng, B.; Xu, L.; Ondráček, M.; Jelínek, P.; Wang, E.; Jiang, Y. Weakly Perturbative Imaging of Interfacial Water with Submolecular Resolution by Atomic Force Microscopy. *Nat. Commun.* **2018**, *9*, 122.

(19) Guo, C. S.; Van Hove, M. A.; Zhang, R. Q.; Minot, C. Prospects for Resolving Chemical Structure by Atomic Force Microscopy: A First-Principles Study. *Langmuir* **2010**, *26*, 16271−16277.

(20) Moll, N.; Gross, L.; Mohn, F.; Curioni, A.; Meyer, G. A Simple Model of Molecular Imaging with Noncontact Atomic Force Microscopy. *New J. Phys.* **2012**, *14*, 083023.

(21) Guo, C.-S.; Xin, X.; Van Hove, M. A.; Ren, X.; Zhao, Y. Origin of the Contrast Interpreted as Intermolecular and Intramolecular Bonds in Atomic Force Microscopy Images. *J. Phys. Chem. C* **2015**, *119*, 14195−14200.

(22) Hapala, P.; Ondráček, M.; Stetsovych, O.; Švec, M.; Jelínek, P. In *Noncontact Atomic Force Microscopy*; Morita, S., Giessibl, F. J., Meyer, E., Wiesendanger, R., Eds.; Springer International Publishing: Cham, 2015; Vol. 3, pp 29−49.

(23) Kawai, S.; Nakatsuka, S.; Hatakeyama, T.; Pawlak, R.; Meier, T.; Tracey, J.; Meyer, E.; Foster, A. S. Multiple Heteroatom Substitution to Graphene Nanoribbon. *Sci. Adv.* **2018**, *4*, No. eaar7181.

(24) Ondráček, M.; Pou, P.; Rozsíval, V.; González, C.; Jelínek, P.; Pérez, R. Forces and Currents in Carbon Nanostructures: Are We Imaging Atoms? *Phys. Rev. Lett.* **2011**, *106*, 176101.

(25) Kawai, S.; Sadeghi, A.; Xu, F.; Peng, L.; Orita, A.; Otera, J.; Goedecker, S.; Meyer, E. Extended Halogen Bonding between Fully Fluorinated Aromatic Molecules. *ACS Nano* **2015**, *9*, 2574−2583.

(26) Shiotari, A.; Sugimoto, Y. Ultrahigh-Resolution Imaging of Water Networks by Atomic Force Microscopy. *Nat. Commun.* **2017**, *8*, 14313.
(27) Jarvis, S. P.; Rashid, M. A.; Sweetman, A.; Leaf, J.; Taylor, S.; Moriarty, P.; Dunn, J. Intermolecular Artifacts in Probe Microscope Images of C60 Assemblies. *Phys. Rev. B: Condens. Matter Mater. Phys.* **2015**, *92*, 241405.
(28) Pavliček, N.; Fleury, B.; Neu, M.; Niedenführ, J.; Herranz-Lancho, C.; Ruben, M.; Repp, J. Atomic Force Microscopy Reveals Bistable Configurations of Dibenzo[a,h]thianthrene and Their Interconversion Pathway. *Phys. Rev. Lett.* **2012**, *108*, 086101.
(29) Pavliček, N.; Herranz-Lancho, C.; Fleury, B.; Neu, M.; Niedenführ, J.; Ruben, M.; Repp, J. High-Resolution Scanning Tunneling and Atomic Force Microscopy of Stereochemically Resolved Dibenzo[a,h]thianthrene Molecules. *Phys. Status Solidi B* **2013**, *250*, 2424−2430.
(30) Lee, A. J.; Sakai, Y.; Kim, M.; Chelikowsky, J. R. Repulsive Tip Tilting as the Dominant Mechanism for Hydrogen Bond-like Features in Atomic Force Microscopy Imaging. *Appl. Phys. Lett.* **2016**, *108*, 193102.
(31) Mönig, H.; Amirjalayer, S.; Timmer, A.; Hu, Z.; Liu, L.; Díaz Arado, O.; Cnudde, M.; Strassert, C. A.; Ji, W.; Rohlfing, M.; Fuchs, H. Quantitative Assessment of Intermolecular Interactions by Atomic Force Microscopy Imaging Using Copper Oxide Tips. *Nat. Nanotechnol.* **2018**, *13*, 371−375.
(32) Mönig, H.; Hermoso, D. R.; Díaz Arado, O.; Todorović, M.; Timmer, A.; Schüer, S.; Langewisch, G.; Pérez, R.; Fuchs, H. Submolecular Imaging by Noncontact Atomic Force Microscopy with an Oxygen Atom Rigidly Connected to a Metallic Probe. *ACS Nano* **2016**, *10*, 1201−1209.
(33) Gross, L.; Mohn, F.; Moll, N.; Meyer, G.; Ebel, R.; Abdel-Mageed, W. M.; Jaspars, M. Organic Structure Determination Using Atomic-Resolution Scanning Probe Microscopy. *Nat. Chem.* **2010**, *2*, 821−825.
(34) Hanssen, K. Ø.; Schuler, B.; Williams, A. J.; Demissie, T. B.; Hansen, E.; Andersen, J. H.; Svenson, J.; Blinov, K.; Repisky, M.; Mohn, F.; Meyer, G.; Svendsen, J.-S.; Ruud, K.; Elyashberg, M.; Gross, L.; Jaspars, M.; Isaksson, J. A Combined Atomic Force Microscopy and Computational Approach for the Structural Elucidation of Breitfussin A and B: Highly Modified Halogenated Dipeptides from Thuiaria breitfussi. *Angew. Chem., Int. Ed.* **2012**, *51*, 12238−12241.
(35) Schuler, B.; Meyer, G.; Peña, D.; Mullins, O. C.; Gross, L. Unraveling the Molecular Structures of Asphaltenes by Atomic Force Microscopy. *J. Am. Chem. Soc.* **2015**, *137*, 9870−9876.
(36) Schuler, B.; Collazos, S.; Gross, L.; Meyer, G.; Pérez, D.; Guitián, E.; Peña, D. From Perylene to a 22-Ring Aromatic Hydrocarbon in One-Pot. *Angew. Chem.* **2014**, *126*, 9150−9152.
(37) Pavliček, N.; Schuler, B.; Collazos, S.; Moll, N.; Pérez, D.; Guitián, E.; Meyer, G.; Peña, D.; Gross, L. On-Surface Generation and Imaging of Arynes by Atomic Force Microscopy. *Nat. Chem.* **2015**, *7*, 623−628.
(38) Pavliček, N.; Mistry, A.; Majzik, Z.; Moll, N.; Meyer, G.; Fox, D. J.; Gross, L. Synthesis and Characterization of Triangulene. *Nat. Nanotechnol.* **2017**, *12*, 308.
(39) Schuler, B.; Zhang, Y.; Collazos, S.; Fatayer, S.; Meyer, G.; Perez, D.; Guitian, E.; Harper, M. R.; Kushnerick, J. D.; Peña, D.; Gross, L. Characterizing Aliphatic Moieties in Hydrocarbons with Atomic Force Microscopy. *Chem. Sci.* **2017**, *8*, 2315−2320.
(40) Schuler, B.; Fatayer, S.; Mohn, F.; Moll, N.; Pavliček, N.; Meyer, G.; Peña, D.; Gross, L. Reversible Bergman Cyclization by Atomic Manipulation. *Nat. Chem.* **2016**, *8*, 220−224.
(41) Kawai, S.; Haapasilta, V.; Lindner, B. D.; Tahara, K.; Spijker, P.; Buitendijk, J. A.; Pawlak, R.; Meier, T.; Tobe, Y.; Foster, A. S.; Meyer, E. Thermal Control of Sequential On-Surface Transformation of a Hydrocarbon Molecule on a Copper Surface. *Nat. Commun.* **2016**, *7*, 12711.
(42) Kocić, N.; Liu, X.; Chen, S.; Decurtins, S.; Krejčí, O.; Jelínek, P.; Repp, J.; Liu, S.-X. Control of Reactivity and Regioselectivity for On-Surface Dehydrogenative Aryl−Aryl Bond Formation. *J. Am. Chem. Soc.* **2016**, *138*, 5585−5593.
(43) Riss, A.; Paz, A. P.; Wickenburg, S.; Tsai, H.-Z.; De Oteyza, D. G.; Bradley, A. J.; Ugeda, M. M.; Gorman, P.; Jung, H. S.; Crommie, M. F.; Rubio, A.; Fischer, F. R. Imaging Single-Molecule Reaction Intermediates Stabilized by Surface Dissipation and Entropy. *Nat. Chem.* **2016**, *8*, 678−683.
(44) Schulz, F.; Ritala, J.; Krejčí, O.; Seitsonen, A. P.; Foster, A. S.; Liljeroth, P. Elemental Identification by Combining Atomic Force Microscopy and Kelvin Probe Force Microscopy. *ACS Nano* **2018**, *12*, 5274−5283.
(45) Mohn, F.; Gross, L.; Moll, N.; Meyer, G. Imaging the Charge Distribution within a Single Molecule. *Nat. Nanotechnol.* **2012**, *7*, 227−231.
(46) Albrecht, F.; Repp, J.; Fleischmann, M.; Scheer, M.; Ondráček, M.; Jelínek, P. Probing Charges on the Atomic Scale by Means of Atomic Force Microscopy. *Phys. Rev. Lett.* **2015**, *115*, 076101.
(47) Sugimoto, Y.; Pou, P.; Abe, M.; Jelínek, P.; Pérez, R.; Morita, S.; Custance, Ó. Chemical Identification of Individual Surface Atoms by Atomic Force Microscopy. *Nature* **2007**, *446*, 64.
(48) Onoda, J.; Ondráček, M.; Jelínek, P.; Sugimoto, Y. Electronegativity Determination of Individual Surface Atoms by Atomic Force Microscopy. *Nat. Commun.* **2017**, *8*, 15155.
(49) van der Heijden, N. J.; Hapala, P.; Rombouts, J. A.; van der Lit, J.; Smith, D.; Mutombo, P.; Švec, M.; Jelínek, P.; Swart, I. Characteristic Contrast in Δf_{min} Maps of Organic Molecules Using Atomic Force Microscopy. *ACS Nano* **2016**, *10*, 8517−8525.
(50) Zint, S.; Ebeling, D.; Schlöder, T.; Ahles, S.; Mollenhauer, D.; Wegner, H. A.; Schirmeisen, A. Imaging Successive Intermediate States of the On-Surface Ullmann Reaction on Cu(111): Role of the Metal Coordination. *ACS Nano* **2017**, *11*, 4183−4190.
(51) Wang, X.-Y.; Richter, M.; He, Y.; Björk, J.; Riss, A.; Rajesh, R.; Garnica, M.; Hennersdorf, F.; Weigand, J. J.; Narita, A.; Berger, R.; Feng, X.; Auwärter, W.; Barth, J. V.; Palma, C.-A.; Müllen, K. Exploration of Pyrazine-Embedded Antiaromatic Polycyclic Hydrocarbons Generated by Solution and On-Surface Azomethine Ylide Homocoupling. *Nat. Commun.* **2017**, *8*, 1948.
(52) van der Heijden, N. J.; Smith, D.; Calogero, G.; Koster, R. S.; Vanmaekelbergh, D.; van Huis, M. A.; Swart, I. Recognizing Nitrogen Dopant Atoms in Graphene Using Atomic Force Microscopy. *Phys. Rev. B: Condens. Matter Mater. Phys.* **2016**, *93*, 245430.
(53) Ebeling, D.; Zhong, Q.; Ahles, S.; Chi, L.; Wegner, H. A.; Schirmeisen, A. Chemical Bond Imaging Using Higher Eigenmodes of Tuning Fork Sensors in Atomic Force Microscopy. *Appl. Phys. Lett.* **2017**, *110*, 183102.
(54) Labidi, H.; Koleini, M.; Huff, T.; Cloutier, M.; Wolkow, R. A.; Pitters, J.; Salomons, M. Indications of Chemical Bond Contrast in AFM Images of a Hydrogen-Terminated Silicon Surface. *Nat. Commun.* **2017**, *8*, 14222.
(55) Hauptmann, N.; Robles, R.; Abufager, P.; Lorente, N.; Berndt, R. AFM Imaging of Mercaptobenzoic Acid on Au(110): Submolecular Contrast with Metal Tips. *J. Phys. Chem. Lett.* **2016**, *7*, 1984−1990.
(56) Grimme, S.; Antony, J.; Ehrlich, S.; Krieg, H. A Consistent and Accurate *Ab Initio* Parametrization of Density Functional Dispersion Correction (DFT-D) for the 94 Elements H-Pu. *J. Chem. Phys.* **2010**, *132*, 154104.
(57) García, R.; Pérez, R. Dynamic Atomic Force Microscopy Methods. *Surf. Sci. Rep.* **2002**, *47*, 197−301.
(58) Boneschanscher, M. P.; Hämäläinen, S. K.; Liljeroth, P.; Swart, I. Sample Corrugation Affects the Apparent Bond Lengths in Atomic Force Microscopy. *ACS Nano* **2014**, *8*, 3006−3014.
(59) Kresse, G.; Furthmüller, J. Efficiency of *Ab-Initio* Total Energy Calculations for Metals and Semiconductors Using a Plane-Wave Basis Set. *Comput. Mater. Sci.* **1996**, *6*, 15−50.
(60) Perdew, J. P.; Burke, K.; Ernzerhof, M. Generalized Gradient Approximation Made Simple. *Phys. Rev. Lett.* **1996**, *77*, 3865−3868.

DOI: 10.1021/acsnano.8b08209
ACS Nano 2019, 13, 786−795